Regular Metal Sulfide Microstructure Arrays Contributed by Ambient-Connected Gas Matrix Trapped on Superhydrophobic Surface

Shasha Wang, Yuchen Wu, Xiaonan Kan, Bin Su, and Lei Jiang**

Controlling the position of metal sulfide architectures is prerequisite and facilitates their device applications in solar cells, light-emitting diodes, and many other optoelectronic fields. Thanks to ambient-connected gas network trapped upon superhydrophobic surfaces, H_2S gas can be continuously transported and reacted with metal ions along solid/liquid/gas triphase contact interface. Therefore, precisely positioning metal sulfide microstructure arrays are generated accordingly. The growth mechanisms as well as influencing factors are investigated to tailor the morphology, structure, and chemical composition of these metal sulfide materials. This interface-mediated strategy can be widely applied to many other metal sulfides, such as PbS, MnS, Ag_2S, and CuS. In particular, heterostructured metal sulfide architectures, such as PbS/CdS concentric microflower arrays, can be generated by stepwise replacement of metal ions inside liquid, exhibiting the advanced applications of this interface-mediated growth strategy.

1. Introduction

Metal sulfides can high-effectively transport photo-generated charge carriers to their surfaces,[1] and therefore have broad technological implications for areas ranging from photocatalysis,[2,3] light-emitting diodes (LEDs)[4] to solar cells,[5] and other optoelectronic applications.[6,7] In order to satisfy the requirement of device applications, position-controlled metal sulfide architectures are prerequisite. Substantial effort has been placed on developing facile methods to generate ordered metal sulfides. Physically high-temperature techniques, such as chemical vapor deposition (CVD)[8–10] and thermal evaporation,[11] have been developed, providing the most effective and versatile approaches to deposit metal sulfides with well-defined structures. Besides these widely used and highly commercialized means of fabrication in semiconductor industry, wet-chemistry synthetic route, especially water/air interfacial reactions between metal ions and H_2S gas,[12,13] has been used as an alternative strategy due to its room-temperature processing feature. Recently, a bubble-template substrate/water/air interface strategy has been explored to induce crystallization occurring along solid/liquid/gas triphase contact lines,[14] rather than traditional liquid/gas biphase counterpart,[12,13] indicating an advanced technique to control the arrangement of final product. However, since the sizes and locations of bubble templates are commonly random, precise positioning of the as-prepared products in above efforts is quite difficult. Therefore, developing an efficient and controllable strategy to prepare precisely positioning metal sulfide architectures should be of great interest and technological importance.

Superhydrophobic surfaces can dramatically repel water due to the existence of a thin air layer trapped inside the gaps of their rough surface microstructures.[15,16] Thanks to this air layer, liquid can be supported by the micropillars, yielding interface-grown golden architectures.[17] By utilizing a three-dimensional microscopic computed tomography (3D-CT) technology, the air pockets have been found to link with each other and form a continuous gas network connected with surrounding ambient. In this case, this atmosphere-connected gas network might not only support liquid but also enable the diffusion and transport of gaseous substance from atmosphere available. Recently, $^1O_2$ gas has been successfully carried and reacted with 9,10-anthracene dipropionate dianion upon superhydrophobic post-arrayed surfaces,[18] indicating the possibility of transporting H_2S gas through the similar way. Furthermore, well-designed pillar-structured superhydrophobic substrates would decide the location of solid/liquid/gas triphase contact interface,[19] allowing precisely positioning interfacial reactions between metal ions and H_2S gas. Accordingly, well-defined metal sulfide architectures can be generated.

Here we demonstrate the interface growth of metal sulfide microstructure arrays upon superhydrophobic pillar-structured substrates. Taking CdS microflower arrays for an example, cadmium source was dispersed in solution supported by

Dr. S. S. Wang, Dr. Y. C. Wu, Dr. X. N. Kan, Dr. B. Su, Prof. L. Jiang
Beijing National Laboratory for Molecular Sciences
Key Laboratory of Organic Solids
Institute of Chemistry
Chinese Academy of Science
Beijing, 100190, PR China
E-mail: subin0000@iccas.ac.cn; jianglei@iccas.ac.cn
Prof. L. Jiang
Key Laboratory of Bio-Inspired Smart Interfacial Science and Technology of Ministry of Education
School of Chemistry and Environment
Beihang University
Beijing 100191, P. R. China

DOI: 10.1002/adfm.201401975

anti-wetting surfaces while sulfur source has been continuously carried by the gas network between solid/liquid interfaces. Owing to preferential growth along solid/liquid/gas triphase interface, CdS grew from the edge of each micropillar, yielding regular CdS microflower arrays. By increasing the external pressure upon the liquid, the growth direction of as-perpared CdS architectures would change from upwards to downwards. With proper concentration, preparation time and temperature, diverse metal sulfides, including PbS, MnS, Ag_2S, CuS microstructure arrays could be generated based on this general superhydrophobic interface strategy. Furthermore, PbS/CdS concentric microflower arrays have been fabricated by stepwise replacement of metal ions inside liquid, indicating the advanced applications of this interface-mediated growth strategy.

2. Results and Discussion

2.1. Fabrication of CdS Architecture Arrays

Photolithographically defined spindle-pillar structured silicon substrate, with typical width 7.5 μm, gap 16 μm, and height 20 μm (**Figure 1**a), have been modified with a thin layer of heptadecafluoro-decyltrimethoxysilane (FAS). Owing to considerable roughness incorporated with low-surface-energy chemical composition, these surfaces showed a superhydrophobic property with a water contact angle of 154 ± 3° (inset in Figure 1a) and contacted with Cd^{2+}-loading solution in H_2S gas atmosphere at room temperature (Figure 1b). After reacting for 20 minutes, regular CdS architecture appeared upon each pillar top while little CdS particles could be found inside pillar gaps (Figure 1c), indicating unique interface growth upon pillar tops rather than pillar bottom regions. Figure 1d and Figure S1 (Supporting Information) reveals the detailed morphology of an individual CdS architecture, showing a bowl-shaped structure with larger top size (long axis: 20.1 ± 2.2 μm, short axis: 16.0 ± 1.7 μm) incorporated with smaller bottom (long axis: 11.0 ± 0.2 μm, short axis: 7.4 ± 0.3 μm). A typical transmission electron microscopy (TEM) observation, as well as the corresponding selected-area electron diffraction (SAED) pattern of a flake taken from the as-prepared CdS microstructures, reveal their crystalline information (Figure 1e). Dispersive diffraction points in the characteristic ring pattern can be respectively indexed as (111), (220), and (311) reflections of cubic phase CdS. The corresponding high resolution TEM (HRTEM) observation (inset image in **Figure 2**a) reveals resolved lattice fringes of (111) planes (d = 0.336 nm). Besides the TEM measurement, XRD analysis (Figure 2a) further confirms the crystallographic structure of as-prepared CdS microstructures. The remarkable enhancement of (111) peak indicates preferential generation of (111) plane in CdS architectures, which is consistent with TEM results. Briefly, interface-induced bowl-shaped architectures are composed of polycrystalline CdS building blocks.

Interface plays an important role in the nucleation and crystallization process. Generally, the concentration of CdS species primarily increases to the critical point, then nucleation occurs in a homogeneous mother liquid bulk.[20] Importantly, the introduction of new interfaces would exert an additional influence on the nucleation of crystals.[21] Similar to the bubble-confined crystallization,[14] superhydrophobic pillar-structured

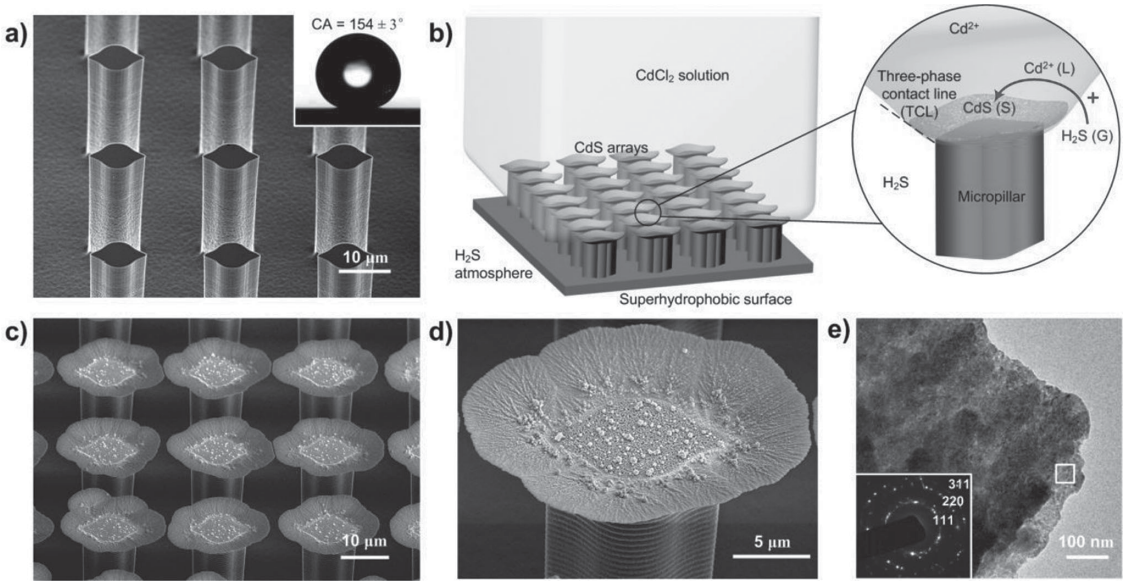

Figure 1. Interface-induced growth of CdS microflower arrays dominated by ambient-connected H_2S network upon superhydrophobic pillar-structured surfaces. a) Side-view scanning electron microscope (SEM) image of a superhydrophobic pillar-structured substrate. The inset image is a photographic view of a 4 μL water droplet upon this surface with a contact angle (CA) of 154 ± 3°. b) Schematic illustration of a superhydrophobic pillar-structured substrate based solid/liquid/gas triphase reaction system. Cadmium source was dispersed in liquid supported by anti-wetting surfaces while sulfur source has been continuously carried by the gas network between solid/liquid interfaces. Owing to preferential growth along solid/liquid/gas triphase interface, CdS grew from the edge of each micropillar, yielding regular CdS microflower arrays. Side-view SEM observations of the as-prepared c) CdS microflower arrays and d) a single interface-mediated CdS architecture (20 min growth). e) A typical TEM image and corresponding SAED pattern (inset image) of a flake taken from the as-prepared CdS microstructure. Dispersive diffraction points in characteristic ring pattern indicate the interface-induced architectures are composed of polycrystalline CdS building blocks.

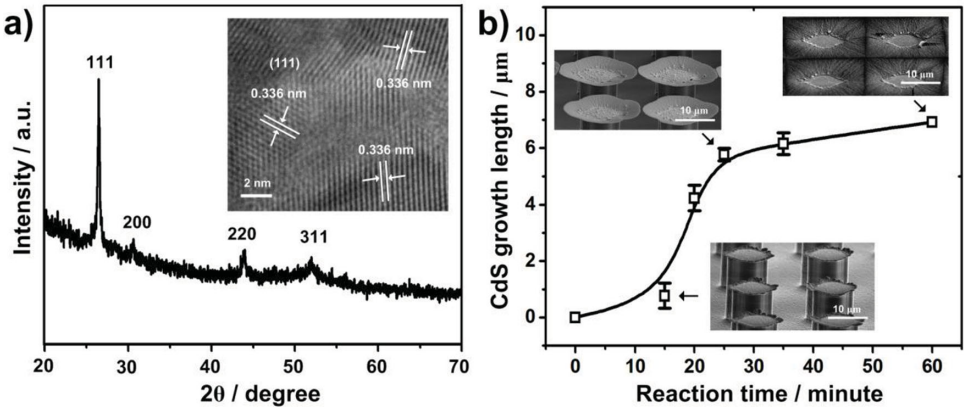

Figure 2. The growth details of CdS architectures upon superhydrophobic pillar-structured surfaces. a) XRD pattern of the as-prepared CdS microflower arrays with remarkable enhancement of (111) peak, indicating preferential generation of (111) plane in CdS architectures. The inset image is HRTEM observation of a flake taken from the as-prepared CdS microstructure, showing lattice fringes of (111) planes (d = 0.336 nm) which is consistent with XRD result well. b) The dependence of edge length of CdS architectures on the reaction time. Inset images are representative SEM observations of CdS microstructures at different growth stages.

substrates in this study generated solid/liquid/gas triphase interface upon each micropillar[17] (Figure 1b), allowing preferential nucleation of CdS along the pillar edges (Figure 1d). As a result, the position of metal sulfide architectures has been well controlled. This interface mediated nucleation and growth process has been proved in Figure S1 (Supporting Information), showing different CdS growth behaviors upon pillar tops (bulk liquid) and along pillar edges (solid/liquid/gas triphase). Compared with randomly dispersed CdS particles upon the flat pillar top (① region in Figure S1, Supporting Information), compact microflower architecture anchored along pillar top edge (② region in Figure S1, Supporting Information). When replacing spindle-shaped micropillars by triangle/circle-shaped ones (Figure S2, Supporting Information), similar results have been observed, indicating the contribution of superhydrophobic surfaces for the preferential nucleation and growth process of CdS architectures.

2.2. Tailoring the Growth Behavior of CdS Architectures

Different experimental parameters have been tailored to investigate their contribution to the interface-mediated CdS growth. The dependence of CdS morphology on reaction time has been studied, shown in Figure 2b and Figure S3 (Supporting Information). At beginning (<15 min), the growth of CdS microflowers proceeded very slowly, indicating a low supersaturation of CdS species inside the Cd^{2+}-loading solution. It should be noted that the CdS growth apparently started from the pillar top edge, which was dominated by solid/liquid/gas triphase interface upon micropillars. Following continuous transport of H_2S gas through ambient-connected gas network upon superhydrophobic surfaces, CdS species in liquid reached a high saturation degree and the crystallization process accelerated, yielding ca. 6 μm CdS edge at 25 min. When reacted for nearly 60 min, CdS microstructures decelerated their growth as they connected with each other, yielding a continuous CdS thin film (Figure S4, Supporting Information). From magnified SEM images, narrow crack junctions with hundreds of nanometers could be found. These cracks were firm evidences that CdS architectures grew from pillar edges then met upon pillar gaps.

The effect of reaction temperature on the growth of CdS architectures has been investigated. Reaction process will be accelerated remarkably when increasing the temperature. However, liquid evaporation rate has been also accelerated, resulting the disappearance of liquid phase as well as the fail of interface-mediated CdS microstructures. Once the reaction environment has been cooled down, no product could be found due to slow reaction process. Therefore, the appropriate reaction temperature should be 15–30 °C, and the effect of temperature in this range on the shapes of CdS microstructures could be negligible.

Since CdS grew along the solid/liquid/gas triphase interface, providing additional external pressure upon liquid bulk would tailor the curvature of solid/liquid/gas triphase interface,[22] thus yielding diverse growth models of CdS architectures, as shown in **Figure 3**. When no external pressure has been applied upon the liquid bulk, solid/liquid/gas triphase interface would perform positive curvature, allowing upward growth of CdS microflowers with an included angle of +27.2 ± 5.6°. Flat CdS architectures grew horizontally by introducing ≈50–75 Pa pressure upon the liquid, indicating curvature change of solid/liquid/gas triphase interface upon pillar tops. Furthermore, under external pressure of ≈100 Pa, the liquid was forced to sink into the gaps between pillars, resulting in a negative curvature of solid/liquid/gas triphase interface. As a result, downward CdS microstructures with an included angle of –48.3 ± 9.2° have been generated accordingly. This interface curvature dominated crystal growth might open a new avenue to control the morphology of products.

2.3. Diverse Metal Sulfide Architecture Arrays

Besides CdS, this interface-mediated strategy could be widely applied to many other metal sulfides via a solid/liquid/gas triphase reaction system. **Figure 4** reveals the SEM images and the corresponding energy dispersive X-ray (EDX) analysis of the pillar-top architectures of PbS, MnS, Ag_2S and CuS. Based on

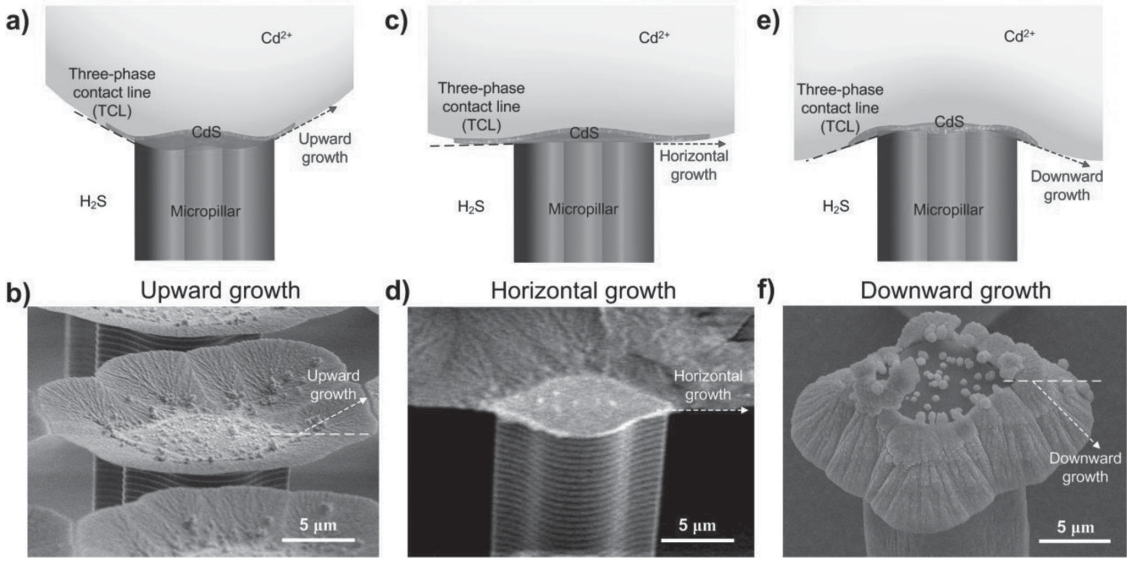

Figure 3. Tailoring the curvature of solid/liquid/gas triphase interface leads to diverse growth models of CdS architectures. The solid/liquid/gas triphase interface can be controlled a) upwards, c) horizontally, e) downwards by introducing 0, ca. 50–75 Pa and ca. 100 Pa external pressure, respectively. Therefore, CdS architectures could grow b) upwards with an included angle of +27.2 ± 5.6°, d) horizontally and f) downwards with an included angle of –48.3 ± 9.2°.

a similar growth process, diverse metal sulfide microstructure arrays have been generated upon micropillar tops. Simultaneously, the presence of individual variations between these metal sulfides depended on the intrinsic crystalline structure of inorganic materials as well as varying experiment parameters. Successful preparation of metal sulfide structures via this interface strategy required low solubility of metal sulfides in liquid solution and a certain reactivity of metal ions and H_2S. Optimum concentration of metal ions and solution pH value initially introduced to the reaction should be well tailored to ensure the growth of metal sulfides (Table S1, Supporting Information).

2.4. Heterostructured Architecture Arrays and Their Optoelectronic Applications

Heterostructured optoelectronic materials are a class of composites that exhibit unique coupled electronic and optical

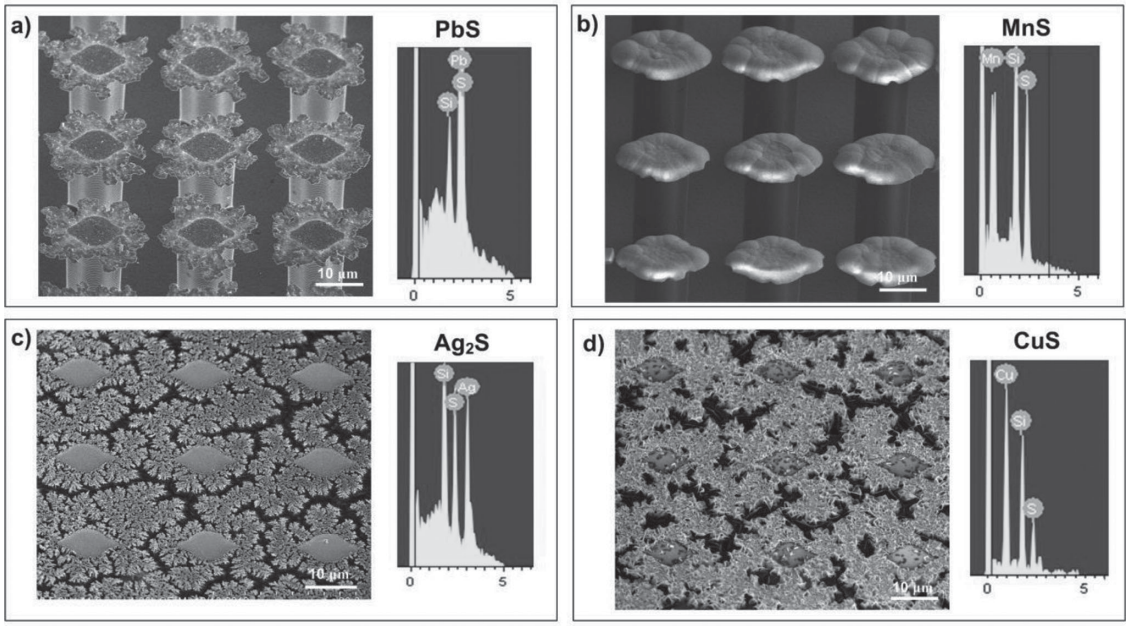

Figure 4. This interface-mediated strategy can be applied to diverse metal sulfides, yielding their regular arrays. Side-view SEM images and the corresponding energy dispersive X-ray (EDX) analysis of a) PbS, b) MnS, c) Ag_2S and d) CuS architectures fabricated via the solid–liquid–gas triphase reaction strategy.

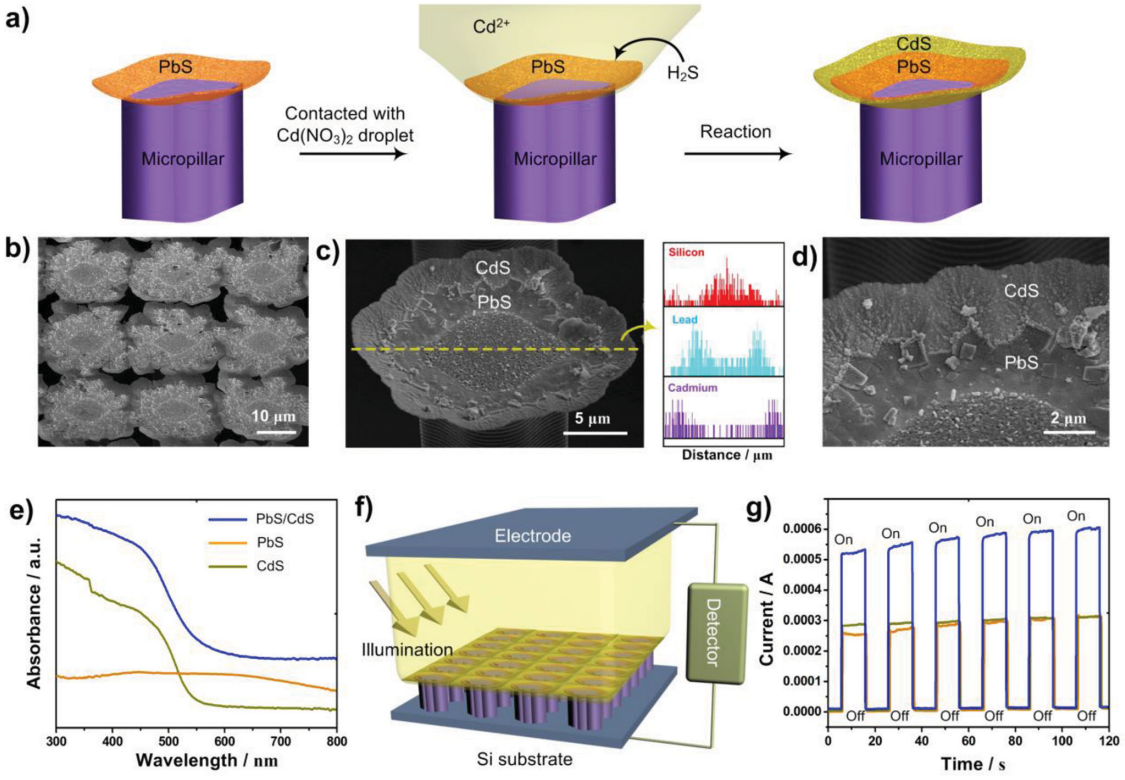

Figure 5. PbS/CdS concentric microflower arrays could be fabricated by stepwise solid/liquid/gas triphase interface reactions with different metal ions in liquid. a) Schematic diagram of the two-step procedure for fabricating heterostructured PbS/CdS architectures. Primarily, PbS microflower arrays have been generated through the interface-mediated strategy. Then, this PbS-loading substrate has been contacted with Cd^{2+}-loading solution in H_2S gas atmosphere, yielding PbS-core/CdS-sheath heterostructured architecture arrays. Side-view SEM observations of the as-prepared b) PbS/CdS concentric microflowers and c) an individual PbS/CdS concentric microflower. The right image in c) is the corresponding linear EDX scan across the pillar-top architectures, indicating gradient distribution of Si, Pb, and Cd elements from center to edge part. d) A magnified image of c), showing an obvious boundary between smooth PbS and rough CdS regions. e) UV–vis absorption spectra of PbS/CdS, PdS and CdS. f) Schematic diagram of the photoelectron-chemical test system. g) The dependence of photocurrent on the irradiation time of PbS/CdS (blue line, 30 min growth of PbS and 30 min growth of CdS), PdS (orange line, 60 min growth) and CdS (dark yellow line, 60 min growth), exhibiting advanced ability of PbS/CdS concentric microstructures compared with individual CdS or PbS counterpart. Photocurrent was recorded under 300 W xenon lamp irradiation ($\lambda \geq 400$ nm) and at a bias potential of 2 V.

properties.[23] In this study, PbS/CdS concentric microflower arrays have been fabricated by stepwise replacement of metal ions inside liquid (**Figure 5**a). Primarily, PbS microflower arrays have been generated through this interface-mediated strategy. Then, this PbS-loading substrate has been endowed with superhydrophobic property by modifying another FAS layer, and contacted with Cd^{2+}-loading solution in H_2S gas atmosphere, yielding PbS-core/CdS-sheath heterostructures. Figure 5b shows regular arrays of PbS/CdS architectures after a two-step interface reaction. Energy dispersive X-ray (EDX) elemental analysis along a line scanning of a single PbS/CdS concentric microflower has been observed in Figure 5c, exhibiting gradient distribution of Si, Pb, and Cd elements from pillar center to edge part. Since a new soild/liquid/gas triphase interface has been generated along PdS microflower edges after the first interface reaction, CdS species would grow along these PbS edges, which can be observed in magnified SEM image in Figure 5d. An obvious boundary between smooth PbS and rough CdS regions can be found, supporting our CdS-edge-growth assumption based on the PbS/ Cd^{2+}-loading-solution/ H_2S interface.

Heterostructure of metal sulfides leads to unique ability in optoelectronic fields. PbS is a attractive semiconductor with a narrow band gap energy and sensitive to near-infrared radiation,[24] while CdS is a visible-light sensitive semiconductor material with high potential in photovoltaics.[25] Here, we demonstrated that the photoelectric conversion capability of PbS/CdS concentric microstructures could be remarkably enhanced due to their co-sensitization effect for the light absorption. Since the growth direction of metal sulfides might yield diverse means of harvesting light, the *I*–*V* characteristics of PbS/CdS architectures with upward (dark yellow line), horizontal (orange line) and downward (blue line) edges have been investigated under the irradiation of a 300 W xenon lamp with cutoff filters ($\lambda \geq 400$ nm), shown in Figure S5 (Supporting Information). Obviously, upward-grown PbS/CdS generated the highest photo-current while the downwards counterparts produced the lowest value. It is well known that curved surfaces would reflect electromagnetic waves depending on their bending angles. The irradiated light would multi-reflect inside upward-grown PbS/CdS architectures, allowing more possibility to harvest photons and the increased current. Differently,

downward structures would reflect the light towards the atmosphere, yielding the poor current value. Therefore, upward metal sulfide structures have been employed in further optoelectronic test.

As shown in Figure 5e, the UV–Vis absorption of the as-prepared PbS/CdS microflower arrays exhibits wider absorption range (300–800 nm) compared with that of individual CdS microstructures (<520 nm), and relatively higher absorption ratio compared with individual PdS microstructures counterpart (especially 300–520 nm). Owing to this improved photon absorbing ability, PbS/CdS microflower arrays showed higher photoelectric conversion capacity. The dependence of photo-responsive current of these three kinds of metal sulfides on time has been investigated at a bias potential of 2 V, shown in Figure 5g. It is obvious that the photocurrent value of PbS/CdS concentric microstructures is about twice compared with that of individual PbS or CdS counterpart, which is contributed by lower recombination of electron-hole pairs, efficient photo-electron emigration, and effective light absorption.[26]

Since a monolayer of low-surface-energy FAS molecules have been induced upon the micropillars to yield anti-wetting property, the influence of this organic layer on the optoelectronic property of PbS/CdS concentric microstructures has been studied. **Figure 6**a exhibits the photocurrent of PbS/CdS microflower arrays before and after the removing of FAS molecules. At the applied voltage of 4 V, the current values are similar to each other, indicating the modification of a FAS monolayer would not change the optoelectronic feature of as-prepared metal sulfide architectures. Furthermore, the chemical/mechanical stabilities of PbS/CdS concentric microstructures have been tested. Neither immersed in 1 mol/L Na_2SO_4 electrolyte for 1–6 days (Figure 6b) nor vibrated in a shaking-bed for 1–3 h (Figure 6c) would change the photocurrent values of as-prepared metal sulfide architectures. Thermo-stable investigation has been performed by heating the PbS/CdS microflower arrays from 25 °C to 100 °C (Figure 6d). The metal sulfides could keep their structure as well as optoelectronic property, showing well temperature-bearing ability.

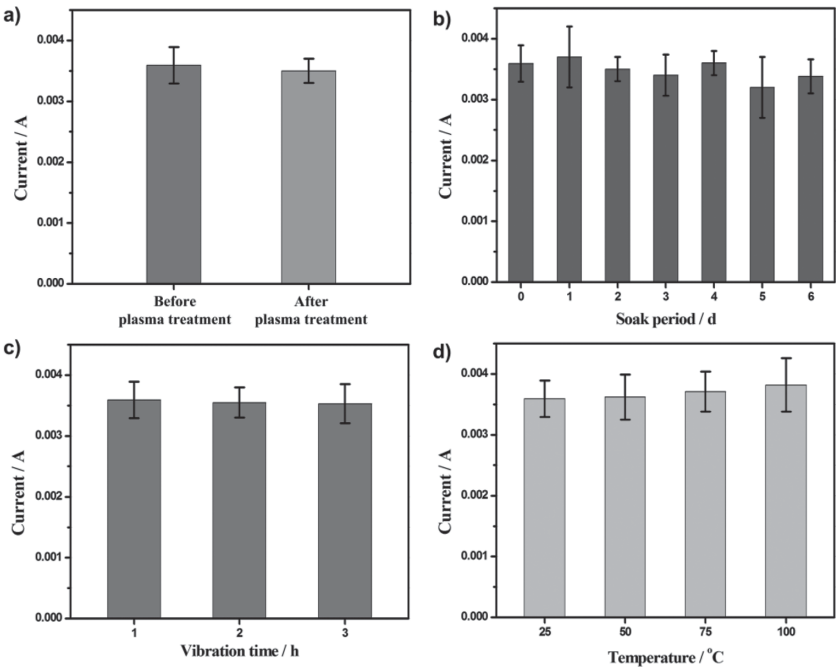

Figure 6. Stable optoelectronic performance of PbS/CdS concentric microflower arrays. a) The photocurrent value of PbS/CdS concentric architectures before and after removing the FAS monolayer. b) The dependence of photocurrent value on the time of soaking metal sulfides in the 1 mol/L Na_2SO_4 solution. c) The dependence of photocurrent value on the time of vibrating metal sulfides at a frequency of 50 Hz. d) The dependence of photocurrent value on the temperature in the heating treatment. As-prepared metal sulfides exhibited well chemical/mechanical/temperature bearing property. All the photocurrents were recorded under 300 W xenon lamp irradiation ($\lambda \geq 400$ nm) and at a bias potential of 4 V.

3. Conclusion

We have developed a general strategy to prepare precisely positioning metal sulfide microstructure arrays through an interface-mediated strategy. This solid/liquid/gas triphase reaction system provided several significant advantageous features for the synthesis of metal sulfide microstructures. First, the growth process could be easily manipulated by solid/liquid/gas triphase intersection, allowing precise reaction sites of final products. Secondly, the synthetic method is a general and flexible process towards a broad range of metal sulfides, as CdS, PbS, MnS, Ag_2S, CuS (Figure 4), and unique microstructures of PbS/CdS concentric microflower arrays (Figure 5). Further investigation of this interface-mediated strategy will be explored to fabricate heterostructured materials including organic-inorganic hybrid materials.

4. Experimental Section

Preparation of Superhydrophobic Substrates: Spindle, triangle or circle-shaped micropillar structured silicon substrates were fabricated via standard photolithography techniques by a direct laser writing apparatus (Heidelberg Instruments DWL200, Germany). The superhydrophobicity of substrates was obtained by silanizing these substrates with heptadecafluoro-decyltrimethoxysilane (FAS) evaporation in a decompression environment at room temperature for 24 h and then heating at 80 °C for 3 h.

Generation of Metal Sulfide Microstructure Arrays: In a typical synthesis, more than 50 μL liquid containing diverse metal salts, such as $Cd(NO_3)_2$, $Pb(NO_3)_2$, $MnCl_2{\cdot}4H_2O$, $AgNO_3$, or $CuCl_2$, was carefully dropped onto 1 cm × 1 cm superhydrophobic pillar-structured substrate in a closed vaccuum dessicator. Owing to anti-wetting property, liquid would be supported by superhydrophobic surfaces, allowing the formation of ambient-connected gas network inside pillar gaps. Then, H_2S gas has been generated and filled the pillar gaps by acidifying Na_2S solution. At proper solution concentration and reaction time (optimum parameters for diverse metal ions can be found in Table S1, Supporting Information), metal sulfides grew from the edge of each micropillar, yielding regular metal sulfide microflower arrays. All the operations were performed at room temperature.

Generation of Heterostructured PbS/CdS Concentric Microflower Arrays: 50 µL liquid of 0.1 M $Pb(NO_3)_2$ was carefully dropped onto 1 cm × 1 cm superhydrophobic pillar-structured substrate in a vaccuum dessicator, and reacted with H_2S gas for 20 min. The Pb^{2+}-loading liquid was removed, allowing as-prepared PbS with superhydrophobic property through another FAS modification. Then, another 50 µL liquid of 0.1 M $Cd(NO_3)_2$ was carefully dropped upon PbS-coated surface, and reacted with H_2S gas for 20 min, yielding PbS/CdS concentric microflower arrays.

Characterizations: The X-ray powder diffraction (XRD) analysis of the samples was performed on a Rigaku X-ray diffractometer with CuKα radiation (λ = 1.54178 Å), the operation voltage and current were maintained at 30 kV and 140 mA, respectively. The morphologies of metal sulfide architectures were viewed by scanning electron microscopic (SEM) (Hitachi, S-4800, Japan) operated at 5 kV. Transmission electron microscopic (TEM) images, high-resolution transmission electron microscopic (HRTEM) images and the selected area electron diffraction (SAED) patterns were recorded on a JEOL-2010 microscope with an accelerating voltage of 200 kV. Samples were collected by sonicating samples in ethanol for 20 min and evaporating upon copper grids for TEM measurements.

Photocurrent Measurements: Photoelectrochemical test systems were composed of a CHI660D electrochemistry potentiostat (Shanghai Chenhua Limited, China), a 300 W xenon lamp with cutoff filters ($\lambda \geq$ 400 nm), and a conventional three-electrode system. The metal-sulfide-loading substrate, Pt plate and Ag/AgCl electrode served as working electrode, counter electrode and reference electrode, respectively. The electrolyte was Na_2SO_4 with a concentration of 1 M.

Chemical/Mechanical/Temperature Bearing Tests: To investigate the chemical stability, as-prepared PbS/CdS concentric microstructure arrays have been immersed in the 1 mol/L Na_2SO_4 solution for 1–6 days. Then, the photoelectrochemical tests have been performed following the above-mentioned process. The photocurrent has been recorded at the applied voltage of 4 V. To investigate the mechanical stability, as-prepared PbS/CdS concentric microstructure arrays have been fixed upon a rigid substrate and vibrated in a shaking-bed for 1–3 h. After that, the photocurrent has been measured at the applied voltage of 4 V. To investigate the temperature stability, as-prepared PbS/CdS concentric microstructure arrays have been heated at 25–100 °C then cooled down to the room temperature. Then, the photocurrent has been measured at the applied voltage of 4 V. To remove the FAS monolayer upon the silicon wafer, the as-prepared PbS/CdS concentric architectures have underwent the oxygen plasma treatment for more than 20 min to ensure the elimination of organics.

Supporting Information

Supporting Information is available from the Wiley Online Library or from the author.

Acknowledgements

S.S.W. and Y.C.W. contributed equally to this work. The authors appreciate the financial support of the National Research Fund for Fundamental Key Projects (2013CB933000), the National Natural Science Foundation (21201169), and the Key Research Program of the Chinese Academy of Sciences (KJZD-EW-M01).

Received: June 16, 2014
Revised: July 13, 2014
Published online: September 5, 2014

[1] a) C. H. Lai, M. Y. Lu, L. J. Chen, *J. Mater. Chem.* **2012**, *22*, 19–30; b) N. F. Zheng, X. H. Bu, P. Y. Feng, *Nature* **2003**, *426*, 428–432.
[2] X. Zong, H. J. Yan, G. P. Wu, G. J. Ma, F. Y. Wen, L. Wang, C. Li, *J. Am. Chem. Soc.* **2008**, *130*, 7176–7177.
[3] a) Y. Hu, X. H. Gao, L. Yu, Y. R. Wang, J. Q. Ning, S. J. Xu, X. W. D. Lou, *Angew. Chem. Int. Ed.* **2013**, *125*, 5746–5749; b) W. T. Sun, Y. Yu, H. Y. Pan, X. F. Gao, Q. Chen, L. M. Peng, *J. Am. Chem. Soc.* **2008**, *130*, 1124–1125.
[4] J. S. Steckel, J. P. Zimmer, S. Coe-Sullivan, N. E. Stott, V. Bulović, M. G. Bawendi, *Angew. Chem. Int. Ed.* **2004**, *43*, 2154–2158.
[5] I. Robel, V. Subramanian, M. Kuno, P. V. Kamat, *J. Am. Chem. Soc.* **2006**, *128*, 2385–2393.
[6] K. J. Wu, K. C. Chu, C. Y. Chao, Y. F. Chen, C. W. Lai, C. C. Kang, C. Y. Chen, P. T. Chou, *Nano Lett.* **2007**, *7*, 1908–1913.
[7] D. V. Talapin, J. S. Lee, M. V. Kovalenko, E. V. Shevchenko, *Chem. Rev.* **2009**, *110*, 389–458.
[8] J. P. Ge, Y. D. Li, *Adv. Funct. Mater.* **2004**, *14*, 157–162.
[9] X. S. Wang, H. B. Feng, Y. M. Wu, L. Y. Jiao, *J. Am. Chem. Soc.* **2013**, *135*, 5304–5307.
[10] X. F. Duan, C. M. Lieber, *Adv. Mater.* **2000**, *12*, 298–302.
[11] X. S. Fang, Y. Bando, G. Z. Shen, C. H. Ye, U. K. Gautam, P. M. Costa, C. Y. Zhi, C. C. Tang, D. Golberg, *Adv. Mater.* **2007**, *19*, 2593–2596.
[12] W. Shenton, D. Pum, U. B. Sleytr, S. Mann, *Nature* **1997**, *389*, 585–587.
[13] H. Bekele, J. H. Fendler, J. W. Kelly, *J. Am. Chem. Soc.* **1999**, *121*, 7266–7267.
[14] D. Aquilano, E. Costa, A. Genovese, F. Massaro, M. Rubbo, *Prog. Cryst. Growth* **2003**, *46*, 59–84.
[15] T. L. Sun, L. Feng, X. F. Gao, L. Jiang, *Accounts Chem. Res.* **2005**, *38*, 644–652.
[16] K. S. Liu, X. Yao, L. Jiang, *Chem. Soc. Rev.* **2010**, *39*, 3240–3255.
[17] Y. C. Wu, K. S. Liu, B. Su, L. Jiang, *Adv. Mater.* **2014**. *26*, 1124–1128.
[18] D. Aebisher, D. Bartusik, Y. Liu, Y. Y. Zhao, M. Barahman, Q. F. Xu, A. M. Lyons, A. Greer, *J. Am. Chem. Soc.* **2013**, *135*, 18990–18998.
[19] a) J. W. Krumpfer, T. J. McCarthy, *J. Am. Chem. Soc.* **2011**, *133*, 5764–5766; b) B. Su, S. T. Wang, J. Ma, Y. L. Song, L. Jiang, *Adv. Funct. Mater.* **2011**, *21*, 3297–3307.
[20] H. Cölfen, M. Antonietti, *Mesocrystals and nonclassical crystallization*, John Wiley & Sons, Chichester, UK **2008**.
[21] I. Kuzmenko, H. Rapaport, K. Kjaer, J. Als-Nielsen, I. Weissbuch, M. Lahav, L. Leiserowitz, *Chem. Rev.* **2001**, *101*, 1659–1696.
[22] A. Lafuma, D. Quéré, *Nat. Mater.* **2003**, *2*, 457–460.
[23] A. Sitt, I. Hadar, U. Banin, *Nano Today* **2013**, *8*, 494–513.
[24] S. M. Lee, Y. W. Jun, S. N. Cho, J. Cheon, *J. Am. Chem. Soc.* **2002**, *124*, 11244–11245.
[25] P. V. Kamat, *J. Phys. Chem. C* **2008**, *112*, 18737–18753.
[26] C. C. Liu, Z. F. Liu, Y. B. Li, J. Ya, E Lei, L. An, *Appl. Surf. Sci.* **2011**, *257*, 7041–7046.